JGR Space Physics

RESEARCH ARTICLE
10.1029/2020JA028942

Development of the Substorm as a Manifestation of Convection Transient

T. Tanaka[1,3], Y. Ebihara[2], M. Watanabe[1], M. Den[3], S. Fujita[4], T. Kikuchi[5], K. K. Hashimoto[6], and R. Kataoka[7]

[1]International Center for Space Weather Science and Education, Kyushu University, Fukuoka, Japan, [2]Research Institute for Sustainable Humanosphere, Kyoto University, Uji, Japan, [3]Space Environment Laboratory, National Institute of Information and Communications Technology, Koganei, Japan, [4]The Institute of Statistical Mathematics, Tachikawa, Japan, [5]Nagoya University, Institute of Space-Earth Environmental Research, Nagoya, Japan, [6]Department of Agriculture, Kibi International University, Minamiawaji, Japan, [7]Space and Upper Atmospheric Group, National Institute of Polar Research, Tachikawa, Japan

Key Points:

- East-west shear inducing the upward field-aligned current at the quiet arc connects from the tail to the ionosphere along the open/close boundary
- The substorm is a manifestation of global reconfiguration of convection system accompanied by the near-earth neutral line (NENL) formation
- The onset starts from the equatorward-most quiet arc since causative narrow shear extends from the NENL along a closed magnetic field

Supporting Information:

Supporting Information may be found in the online version of this article.

Correspondence to:

T. Tanaka,
takashi.tanaka.084@m.kyushu-u.ac.jp

Citation:

Tanaka, T., Ebihara, Y., Watanabe, M., Den, M., Fujita, S., Kikuchi, T., et al. (2021). Development of the substorm as a manifestation of convection transient. *Journal of Geophysical Research: Space Physics*, *126*, e2020JA028942. https://doi.org/10.1029/2020JA028942

Received 23 NOV 2020
Accepted 10 SEP 2021

Abstract We reproduced the substorm by global simulation and analyzed the development of convection, shear, the dynamo, and the field-aligned current (FAC) at the final stage of the growth phase. From these investigations, we show that the substorm is a manifestation of reconfiguration in global flow dynamics. Ionospheric convection can be understood from two aspects. One understanding is as the potential field generated by the FAC, and the other is as the projection of magnetospheric convection. In order for the two to coincide, the FAC must be transmitted together with the motion. As a consequence, the resulting convection must be continuous from the magnetosphere to the ionosphere. We see this connection from the drawing of shear to recognize that the substorm is the projection process of transient convection. In the growth phase, convective shear that causes the quiet arc and the Harang reversal (HR) occurs on the open/closed boundary along the surface of the plasma sheet with a continuous flow structure from the magnetosphere to the ionosphere. The onset starts from a more local flow that is induced by the near-earth neutral line (NENL). A narrow shear commences from the NENL in the mid-tail and extends to the ionosphere to replace growth phase shear. Along a closed magnetic field line connected to the NENL, direct penetration flow, squeezing flow, the near-earth dynamo, release of the HR, and the onset FAC occur successively and consequently cause the ground onset. Such onset mechanism is quite different from the model adopting the current wedge.

1. Introduction

The field-aligned current (FAC) is an essential factor in generating the substorm sequences. It is a major theme of substorm research to elucidate the origin of the upward FAC in the quiet arc during the growth phase (Coroniti & Pritchett, 2014; Jiang et al., 2012; Sergeev, Nishimura, et al., 2012), and the upward FAC which causes the initial brightening at the onset (Kepko et al., 2015; Sergeev, Angelopoulos, et al., 2012). Among them, how the onset FAC is generated is the most prominent issue in the substorm research. It is an absolute understanding in observational models that the upward FAC causing the onset is generated from the current wedge (CW) (Kepko et al., 2015; Liu et al., 2015). At the same time, some global simulations have reproduced the distribution of the FAC during the substorm and given solutions that seem to confirm the CW (Nishimura & Lyons, 2016; Raeder et al., 2001; Yu et al., 2017).

Under such circumstances, it has been found out recently that if we increase the resolution of the simulation in the ionosphere then we can obtain an onset solution different from the CW (Tanaka, Ebihara, et al., 2017, Tanaka et al., 2021). The point of this model is symbolized in the near-earth dynamo (Ebihara & Tanaka, 2015b). This result brings to light the deficiency of the CW that the underlying concept of the CW lacks the important role of the FAC in transmitting motion. Generally, the mechanical effect of the FAC is to transmit field-perpendicular motion (Iijima, 2000; Tanaka, 2007) between the magnetosphere and the ionosphere. The globally orderly configuration of the region-1 and region-2 FACs (Iijima & Potemra, 1976) indicates that the FAC is transmitting global convection. The purpose of this paper is to see how the FAC and motion interrelate in transmitting substorm disturbances from the tail to the ionosphere.

In this paper, we further relate the substorm FAC with flow dynamics, adopting the flow field of our magnetohydrodynamics (MHD) solution. Investigations are done by coupling the FAC with magnetospheric shear structure. This is the problem of connecting the substorm FAC from the magnetosphere to the ionosphere. It is considered throughout this study including during the substorm that the FAC occurs first with an attempt to transmit motion and particle precipitation occurs as a consequence (Iijima, 2000; Tanaka, 2007). In this study, particle precipitation is not the cause of the FAC.

1.1. Generation of the FAC

Since the role of the FAC is to transmit field-perpendicular motion, its coupling with the momentum equation is quite natural. By calculating the divergence of field-perpendicular current from the momentum equation, we can see one aspect of the FAC generation (Sato & Iijima, 1979; Vasyliunas, 1970). To be precise, this is a conversion process from field-perpendicular current to field-parallel current. As a result of these analyses, conversion conditions are derived such as time variation of vortex motion and the non-parallelism of contour lines of pressure P and strength of magnetic field $|B|$. This theory explains the relationship between the generation of the region-2 FAC and the high-pressure region at the inner edge of the plasma sheet (Vasyliunas, 1970; Watanabe et al., 2019). Around there, the ionospheric FAC can be estimated from these laws, because a simple field-parallel integration is applicable along a relatively short closed magnetic field line.

The ionosphere is a dissipative region, therefore the generation of the FAC needs to be accompanied by the generation of electromagnetic energy. This situation provides another approach to the FAC generation that the formation of dynamos is indispensable in the magnetosphere. The global simulations have succeeded to show concretely the coupling structure between the FAC, the dynamo, and convection (Tanaka, 1995, 2007; Tanaka et al., 2016; Watanabe et al., 2019). In the global simulation, the dynamo ($J \bullet E < 0$) is the energy source of the FAC in all cases of the northward interplanetary magnetic field (IMF), the growth phase, and the onset. Principally, the origin of convection is the solar wind-magnetosphere interaction, which causes a fraction of solar wind energy to penetrate into the magnetosphere. Overall, convection is the process to discharge this energy from the magnetosphere (Tanaka, Obara, et al., 2019).

Considering a viscous interaction between the solar wind and the magnetosphere, the dynamo ought to be at the low-latitude boundary layer. In this case, the dynamo is driven by viscous force. Viscosity generates dynamo energy by slowing down the solar wind penetrating from the flank (Johnson & Wing, 2015). In the case of solar wind-magnetosphere interaction due to the dayside reconnection, on the contrary, deceleration of the magnetosheath flow (Wilder et al., 2015) or the cusp-mantle dynamo (Tanaka et al., 2016) should be the origin of the FAC. The former produces the FAC by converting motional energy to electromagnetic energy and the latter produces the FAC by converting internal energy to electromagnetic energy. In the cusp-mantle dynamo, the slow-mode motion acts to convert internal energy to electromagnetic energy (Tanaka et al., 2016; Watanabe et al., 2019), and the main discharging route of penetrated energy is downstream emission of plasma via the mantle (Tanaka, Obara, et al., 2019). Energy conversion is built into this path, causing the FAC and ionospheric convection. As a result, a part of penetrated energy is discharged also to the ionosphere. The mechanism of conversion from internal energy to electromagnetic energy is valid even in the substorm case treated in this study.

Energy is transmitted in the space around the FAC, where energy propagates as pointing flux (Ebihara et al., 2019; Kikuchi, 2014). Therefore, the FAC itself does not bear energy transfer. The dynamo is a source of pointing flux. However, the dynamo is essential not only for energy conversion but also for the conversion of field-perpendicular current to field-parallel current (Watanabe et al., 2019). This is also referred to as the coupling of the slow mode and the Alfven mode. Thus, the transfer of momentum by the FAC and the conversion of energy by the dynamo are essential elements for magnetosphere-ionosphere (M-I) convection.

1.2. FAC and Shear

Next, we consider the process by which the FAC is connected to the ionosphere. From the induction equation

$$\nabla \times \mathrm{E} = -\frac{\partial B}{\partial t}, \tag{1}$$

and, current equation

$$\nabla \times \mathrm{B} = \mu_0 J, \tag{2}$$

we can obtain the relationship between the FAC and the electric field (motion) as

$$\frac{\partial J_{\parallel}}{\partial t} = -\frac{1}{\mu_0}\left(\nabla \times \nabla \times E\right)_{\parallel}. \tag{3}$$

After modifying Equation 3, we obtain

$$\frac{\partial J_{\parallel}}{\partial t} = -\frac{1}{\mu_0}\left(\nabla\left(\nabla \cdot E\right) - \Delta E\right)_{\parallel}. \tag{4}$$

Considering the low-altitude region away from the source region, we can assume $(\Delta E)_{\parallel} = \Delta E_{\parallel}$ since the curvature of magnetic field lines is small. Then we can obtain from Equation 4

$$\frac{\partial J_{\parallel}}{\partial t} = -\frac{1}{\mu_0}\nabla_{\parallel}\left(\nabla_{\perp} \cdot E_{\perp}\right) \tag{5}$$

(Song & Lysak, 2001). This equation shows that charge distributes uniformly along magnetic field lines. Here, in the MHD, $E_{\parallel} = 0$. $(\Delta E)_{\parallel}$ is a term indicating the place where FAC tracing and magnetic field tracing begin to deviate. When the FAC is sheet-like and flat, we can obtain

$$\nabla_{\perp} \cdot E_{\perp} = -\mathrm{B} \cdot \left(\nabla \times \mathrm{V}\right) + \mathrm{V} \cdot \left(\nabla \times \mathrm{B}\right), \tag{6}$$

which means that shear must continue from the magnetosphere to the ionosphere when the FAC is additionally supplied from the source region to the ionosphere. That is, convection shear must be transmitted to the ionosphere along with the FAC. In the quasi-steady state after the increase of the FAC, shear will also exist continuously as it is. Here, the second term on the right side of Equation 6 is small at low altitudes. In this way, the FAC and shear coexist in both the developing stage and the quasi-steady state. Therefore, the structure of the FAC should overlap with shear structure, which is a part of the convection. Convection needs to not only exist in the magnetosphere but also lead to the ionosphere. Thus, magnetospheric convection, the FAC, shear, and ionospheric convection are expected to coexist as an integrated structure.

1.3. FAC During the Substorm

In general, the intensity of the FAC increases with increasing activity of magnetic field (Iijima & Potemra, 1976). The FAC strengthens its magnitude in the substorm growth phase and the subsequent expansion phase. To know the origin of the upward FAC in the quiet arc that characterizes the growth phase may be essential as a prerequisite for elucidating the onset. In the conventional interpretation, the quiet arc is caused by scattering of plasma sheet particles due to enhanced curvature of plasma sheet magnetic field under the thinning condition (Sergeev, Nishimura, et al., 2012). In other words, it is an interpretation that looks upon particle precipitation as the primary cause of the FAC. Here, convection acts a role to carry the magnetic field and cause the plasma sheet thinning. That is, convection is regarded only as a deformation process of the magnetospheric magnetic field. Here, the FAC is the result of particle precipitation. As a result, the FAC does not link with motion, and there arises no need to consider the dynamo or energy conversion.

Coroniti and Pritchett (2014) attributed the quiet arc to the upward FAC. In their model, the origin of the FAC is the non-parallelism of contour lines of P and $|B|$ in the plasma sheet. In the global simulation by Tanaka, Ebihara, et al. (2017) and Tanaka et al. (2021), the same perspective of relating the quiet arc to the FAC appears also. In this case, however, the upward FAC is associated with shear at the lobe/plasma sheet boundary. The current line tracing from the quiet arc first passes through shear, and then eventually reaches the mantle. Thus, the cusp-mantle dynamo supplies energy to the quiet arc. At this time, convection returns to the dayside through the vicinity of the lobe/plasma sheet boundary without reaching the center of the plasma sheet. At the same time, the projection of this convection produces the Harang reversal (HR). In the understanding of the quiet arc by particle scattering, the quiet arc and the HR are explained separately. The HR is explained as the deflection of plasma sheet convection (Ohtani et al., 2016). Among the global simulations, only Tanaka et al. (2021) reproduced both the quiet arc and the HR simultaneously as a part of global convection. It is a large difference between the conventional interpretation and the global simulation

that the high-latitude side of the quiet arc is on a close magnetic field in the former but this part is on an open magnetic field in the latter.

Next, we must consider how the FAC that causes the onset is generated. In the traditional model, the CW plays a leading role at this stage in place of particle scattering in the growth phase. That is, it is an absolute understanding in the traditional model that the upward FAC causing the initial brightening is generated from the CW (Liu et al., 2015; Sergeev, Angelopoulos, et al., 2012). The mechanism of the CW generation is explained by the sequence of the near-earth neutral line (NENL), the bursty bulk flow (BBF), instability, and the CW. Here, the CW is triggered by instability due to external stimulation (BBF), but there is another understanding that it is by spontaneous instability (Lui et al., 2008). In this case, the sequence is reversed. Traditionally, the NENL most often originates from antiparallel reconnection (McPherron, 2016). In this model, thinning is a necessary condition for the NENL.

Many global simulations have reproduced the NENL-BBF-CW sequence (McPherron et al., 2020; Nishimura & Lyons, 2016; Pham et al., 2016; Raeder et al., 2001; Sorathia et al., 2020; Yu et al., 2017). Some of these papers also presented the onset FAC in the ionosphere. In these results, however, the FAC calculated in the ionosphere appears to be still insufficient for detailed inspections of the onset mechanism. In addition, the CW is seldom confirmed from the current line tracings. Nevertheless, these papers concluded that the ground onset is induced by the CW.

In the high-resolution global simulations studied by us, the formation of the near-earth dynamo is the cause of initial brightening, instead of the traditional CW (Ebihara & Tanaka, 2015b; Tanaka, Ebihara, et al., 2017). Due to the magnetic tension released from the NENL, a high-pressure region P is formed in the inner magnetosphere away from the equatorial plane (Yao et al., 2015). Simultaneous with the NENL formation, the path of return convection changes from the O/C boundary to the center of the plasma sheet. At the same time, the field-perpendicular motion $V_{\perp}$ linked to the NENL is generated on the magnetic field line connected to the NENL. In this way, the near-earth dynamo, the region of $J \bullet E < 0$, occurs on a field line linking with the NENL. Here, J and E are given by $J \times \mathrm{B} = \nabla \mathrm{P}$ and $E + V \times B = 0$. In the global simulation, the NENL generation is not antiparallel reconnection, but a guide field reconnection coupled with the evolution of the magnetic topology (Tanaka, Ebihara, et al., 2019, Tanaka et al., 2021). In this topology, guide field reconnection occurs between two closed field lines connected to retreating nulls in the remnant of the null-separator structure under the northward IMF.

Traditionally, shear associated with the BBF has been considered in the equatorial plane. Occasionally, this shear is understood as the dynamo (Birn & Hesse, 2013). However, shear must be the FAC guide, not the dynamo. Regardless of whether the near-earth dynamo or the CW, shear connection to the ionosphere is necessary to maintain the FAC. Even when considering shear on the equatorial plane associated with the CW, however, motion that accompanies the FAC is scarcely considered between the CW and the ionosphere. Some researchers believe that projections of the NENL and the BBF are observable even in the ionosphere (Lyons et al., 2021). But the global simulations do not reproduce such projection (Tanaka, 2015). This is because the projection region of the plasma sheet onto the ionosphere becomes extremely narrow before the onset. In this way, there are still many inconsistent parts in the relation between the flow structure and generation of the onset FAC. Overall, the coexistence structure of the FAC and shear is not accurately recognized, regardless of its clear existence from a mathematical model (Equation 5). The CW tends to take us away from the complicated understanding of the onset based on the global dynamics since the CW enables us to understand the onset only from the local structure. It is the subject of this paper to improve these understandings. It will be shown from these investigations that the substorm seen from the global simulation provides another way of understanding the substorm.

2. Numerical Model

The calculation in this paper applies parallelized high-resolution M-I coupling model REProduce Plasma Universe (REPPU) code. Details of the REPPU code were shown in Tanaka, Ebihara, et al. (2017). In this code, the solar wind-magnetospheric region is calculated by the MHD model. The calculation area is from 3 Re to 300 Re in the radial distance. High resolution is achieved by using the triangular grids that are obtained by dividing from a dodecahedron. This system can avoid accumulation points in the grid system

(Nakamizo et al., 2009). Total grid number is 71,271,560. Among them, 122,882 grids are allocated on the inner boundary. A visualization of this grid system is observable in the Supporting Information of Tanaka et al. (2020). Spatial discretization is done by the finite volume total variation diminishing scheme (Tanaka, 1994, 1995). For reference, the number of grids is 0.16 million in Pham et al. (2016), 1.3 million in Nishimura and Lyons (2016), and 74 million in Sorathia et al. (2020).

In the ionosphere, a potential model is solved from the ionospheric Hall and Pedersen currents and the FAC. Electric conductivity is a function of the solar zenith angle, the FAC, pressure, and temperature (Tanaka, 2000). The MHD model and the potential model mutually exchange the FAC and the potential to form the M-I coupling system. Between 1 Re and 3 Re, physical variables are projected along the dipole. The most important advantage of this code is that it realizes high-resolution calculation not only in the magnetosphere but also in the ionosphere. The direction of the X axis is toward the sun, the direction of the Y axis is toward opposite to the earth's orbital motion, and the direction of the Z axis is toward the north.

In the substorm simulation, it is inevitable to set an initial condition. This is the magnetosphere under the northward IMF condition. For that reason, we first generate a quasi-stationary magnetosphere under the obliquely northward IMF. ($\rho = 5$/cc, $Vx = -370$ km/sec, $By = -2.0$ nT, $Bz = 4.0$ nT, $T = 34{,}000$). This quasi-stationary structure is characterized by the 2-null 2-separator structure. This solution under the northward IMF gives not only the initial condition of the substorm but also reproductions the sun-aligned arc, the fan-shaped arc, and the theta aurora, confirming the authenticity of the model (Tanaka, Obara, et al., 2017, Tanaka, Obara, et al., 2019; Tanaka et al., 2018). Through studies of these structures under the northward IMF, we have got a general conclusion that the solar wind-magnetosphere interaction takes place through the null-separator structure. Next, the IMF is changed to obliquely southward ($Bz = -4.0$ nT) to generate a medium-scale substorm. Here in this paper, the case of IMF $By < 0$ is treated. As a supplementary explanation, the MHD simulation cannot accurately calculate the case of IMF $Bz < -10$ nT. This is because $P_{\perp} > P_{\parallel}$ cannot be calculated for the inner magnetosphere. Therefore, the magnetic storm cannot be reproduced only by the MHD. However, the MHD simulation is effective for the reproduction of the medium-scale substorm, because IMF $Bz < -10$ nT is not required for the substorm.

Contrary to the expectation that the substorm onset is mainly a manifestation of the non-MHD process, the present simulation reproduces the substorm onset even with a simple viscous model, provided that the MHD simulation has advanced to a high-resolution version that calculates accurate M-I coupling (Ebihara & Tanaka, 2015a, 2015b, 2016, 2017; Ebihara et al., 2014, 2019; Tanaka, 2015; Tanaka, Ebihara, et al., 2017, 2019; Tanaka et al., 2010, 2020, 2021). This result indicates that correct reproduction of the global configuration that satisfies the precondition for the reconnection is more important than accurate evaluation of non-MHD effects itself. That is, understanding of the substorm onset mainly considering the NENL and the CW is still insufficient to clarify the onset.

Satellite observations have revealed typical changes in the magnetosphere during the substorm. These are the plasma sheet thinning and enhancement of the lobe field in the first stage, the NENL, the BBF, the dipolarization front (DF) in the second stage, the dipolarization, and the D-deflection in the expansion phase. The global simulation used in this paper reproduces these variations as shown before (Tanaka, Ebihara, et al., 2017; Tanaka et al., 2010). The present simulation can be an important research tool for the substorm, because it can draw structures that can never be obtained from observations, such as tracings of magnetic field lines, current lines, and streamlines, and the null separator structure (Tanaka, Ebihara, et al., 2019).

The credibility for the present solution of numerically generated substorm can be confirmed more directly, by comparing numerical solutions with ionospheric observations such as the AU/AL variations (Tanaka et al., 2020) and auroral disturbances estimated from the FAC (Ebihara & Tanaka, 2015a; Tanaka, Ebihara, et al., 2019; Tanaka et al., 2021). The simulation reproduces overall features of ionosphere disturbances that have been known for a long age. The problem here is to know what magnetospheric structure corresponds to these ionospheric events and how the M-I coupling system transmits them to the ionosphere. In this study, we mainly try to clarify the magnetospheric shear structure that couples the FAC development in two regions.

3. Results and Discussion

In the solution analyzed in this study, the growth phase lasts for about 1 hr after the southward turning of the IMF, and then the NENL occurs in the equatorial plane of the tail at $T = -2.8$ min. Time is taken as the onset on the ground is at $T = 0$ min. The NENL occurs at $X = -17.5$ Re and at LT 23 before midnight. Here, we call the growth phase interval until the NENL onset the first stage, and the period from the NENL onset to the ground onset the second stage. Although details are not presented in this paper, the first stage of the growth phase proceeds under the conditions that the shape of the magnetic field changes but the null distribution keeps a constant structure (Tanaka, Ebihara, et al., 2019). At the NENL onset, the NENL occurs as guide field reconnection with the appearance of a new null. This reconnection occurs between two different closed magnetic field lines. The second stage begins with the occurrence of the NENL, then various fluctuations follow in the near-earth tail region. The onset on the ground ($T = 0$ min) starts 2.8 min after the occurrence of the NENL. In this study, the onset in the northern ionosphere occurs in the evening convection cell at 23 LT (Tanaka, Ebihara, et al., 2019; Tanaka et al., 2021). This result depends on the negative IMF By. From the AU/AL magnitude, the numerically reproduced substorm is a medium-scale one. Above appearances of the simulated substorm have already been reported by Tanaka, Ebihara, et al. (2017, 2019) and Tanaka et al. (2020, 2021).

Developments of the M-I coupling system from the growth phase to the onset were already reported in many previous studys. The development of the ionospheric FAC was reported by Tanaka, Ebihara, et al. (2017, 2019) and Tanaka et al. (2010, 2021). To avoid duplication, we show the summary of this result by Movie M1 in the Supporting Information. See the previous studys for more details on the variations seen here. Details may differ between former and present papers, but this difference does not affect discussions of the present study. Developments of plasma pressure and velocity were reported by Tanaka, Ebihara, et al. (2017), Tanaka et al. (2010). Movie M2 in the Supporting Information shows the development of pressure in the noon-midnight meridian plane. Change of magnetic topology in the magnetosphere from the growth phase to the onset was reported by Tanaka, Ebihara, et al. (2019) and Tanaka et al. (2010, 2021). We can see null structure affecting the substorm processes.

We newly present in this study a three-dimensional structure of shear and its relation to the FAC, which connects the dynamo and the ionosphere. Considering div $J = 0$ and Equation 6, it is expected that $J_{\parallel}/|B|$ and $B \bullet$ rotV will be constant along a field line in the low-altitude region. If we examine $B \bullet$ rotV directly, however, it becomes relatively small in the magnetosphere and relatively large in the ionosphere. Since magnitudes vary so much, it is difficult to display them throughout the entire region at the same time. These deviations from $B \bullet$ rotV constant along a field line may appear in shear structure since the actual solution includes some non-ideal effects. Therefore, here in this study, we display $B \bullet$ rotV/sqrt ($|B|$). This value is quite appropriate to display the result uniformly from the middle tail to the ionosphere.

In this study, the + layer is clockwise shear, and the − layer is counterclockwise shear seeing toward the magnetic field lines. Considering the structure in which the dynamo is on the magnetospheric side, the + layer corresponds to the upward FAC and the − layer corresponds to the downward FAC in the northern hemisphere. Similarly, in the southern hemisphere, the + layer corresponds to the downward FAC, and the − layer corresponds to the upward FAC.

3.1. Before the NENL Onset (First Stage)

Figure 1 shows shear and FAC structures just before the end of the first stage ($T = -5.6$ min). Here, colors illustrate the distribution of the FAC at 3 Re. In the northern hemisphere, the blue color indicates antiparallel to magnetic field lines (upward component), and red color indicate parallel to magnetic field lines (downward component). Figure 1 mainly shows the evening side where the high-latitude side is blue and the low-latitude side is red. The inset in the left bottom part shows the FAC distribution seen from the north. After midnight in the ordinary case, the high-latitude side should be red and the low-latitude side should be blue. In Figure 1, however, these blue (high latitude) and red (low latitude) areas extend from before midnight to past midnight even as far as the morning side. This is the characteristic structure for the growth phase under IMF *By*− (Tanaka, 2015; Tanaka, Ebihara, et al., 2019, Tanaka et al., 2021). We will call the FAC

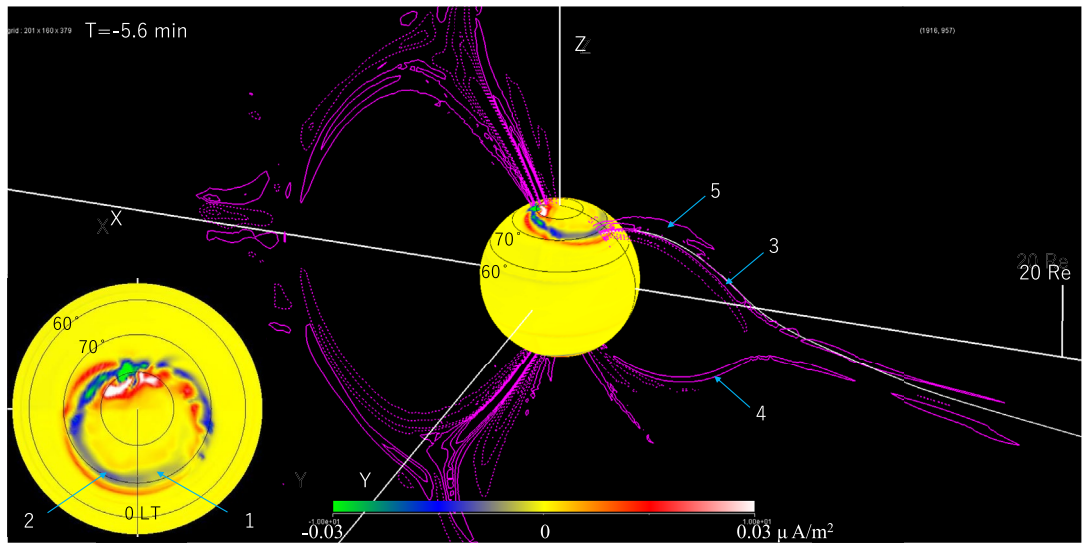

Figure 1. Shear structures in the 12 LT and 23 LT meridian planes at the late growth phase at $T = -5.6$ min (magenta contour). Solid and dashed contours illustrate + and − layers, respectively. Contour interval is $2.5*10^{1/2}/120$ $(nT)^{1/2}$/sec. Color shadings show the FAC on the 3 Re spherical surface. Black circles show projected ionospheric latitudes. Upward FAC (blue) in the northern hemisphere is extending from the evening across the midnight as far as the morning region. A white line shows the first open field line in the 23 LT meridian. Inset in the left bottom part shows the FAC distribution seen from the north. See encircled numbers in the text for the meaning of numbers.

part beyond midnight the extended part①. On the other hand, the part before midnight is called the normal part②. In the southern hemisphere, the extended part occurs before midnight.

Contour lines in Figure 1 show shear distributions in 12 LT (noon) and 23 LT (before midnight) meridian planes. Solid lines illustrate the + layer, and broken lines illustrate the − layer. The most prominent shear is the + layer in the northern hemisphere③, which corresponds to clockwise vortex toward field lines, that is, toward the earth. Seen from the ionosphere, the + layer in the northern hemisphere is connected to the upward region-1 FAC. As shown by Tanaka (2015) and Tanaka et al. (2021), this FAC structure represents the region corresponding to the quiet arcs. This area is also the place where the onset will start soon after. It was also shown by Tanaka (2015) and Tanaka et al. (2021) that the upward FAC from the quiet arc in the growth phase also extends deep into the tail, and finally reaches the cusp-mantle dynamo. It can be seen from Figure 1 that the + layer in the northern hemisphere continues from the middle tail to the ionosphere. Therefore, the FAC structure connecting the dynamo and the quiet arc is consistent with extending + shear layer in Figure 1. The FAC extending from the tail to the quiet arc is realized from + shear layer in Figure 1 through Equation 5. Field-perpendicular current from the cusp-mantle dynamo changes to the FAC at the place where $(\Delta E)_{\parallel}$ term is effective in Equation 4.

The + layer in Figure 1 in the southern hemisphere④ corresponds to the extended part of the region-2 FAC that is equatorward of the extended part of the region-1 FAC. In the evening in the southern hemisphere, the − layer corresponds to the normal part of the downward region-2 FAC. In the southern hemisphere, 23 LT is near the boundary between the normal part and the extended part. In this local time, structure in the southern hemisphere becomes more complicated than in the northern hemisphere, and the southern + layer is not a counterpart of the northern + layer. In the tail, however, the northern and southern + layers appear to approach each other across the plasma sheet. The appearance of connection from the tail to the ionosphere is similar for the + layers in the northern and southern hemispheres. The shape is almost symmetrical. This feature is expected to correspond to the thinning of the plasma sheet. Shear layer continuing from the tail to the ionosphere is a part of the global convection structure. It can be expected from Figure 1 that the FAC connects to the ionosphere together with convection shear.

A white line in Figure 1 shows the first open magnetic field line at this local time. In the northern hemisphere, the + layer extending from the mid-tail to the ionosphere is almost on or slightly outside this

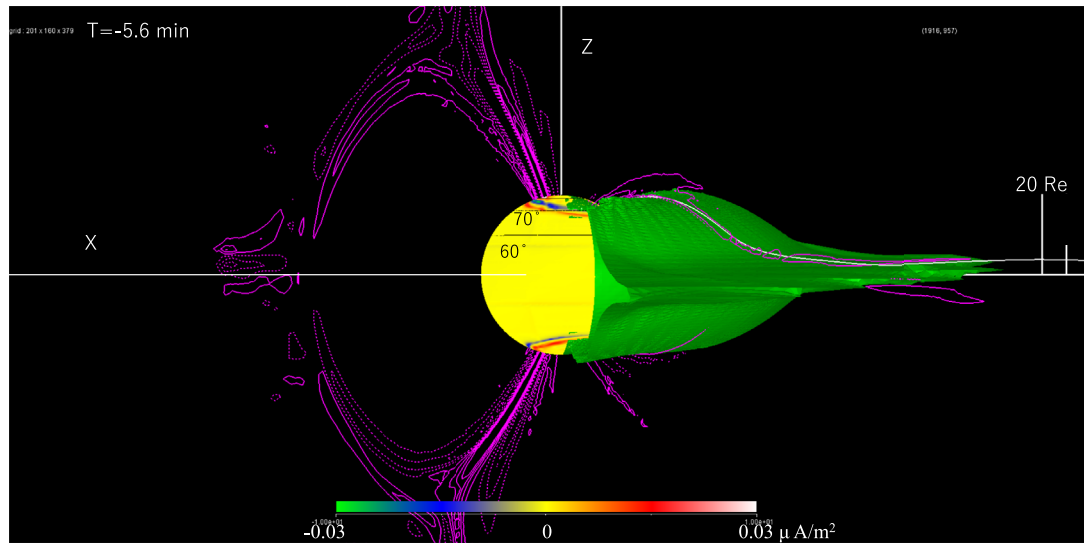

Figure 2. The same drawing as Figure 1 but with an additional contour surface of pressure showing the plasma sheet at the late growth phase (green). The contour surface is drawn for 0.1 nP in 20-04 LT. Color shadings show the field-aligned current on the 3 Re spherical surface. A white line shows the first open field line in the 23 LT meridian. The view is from a slightly night side in the equatorial plane.

magnetic field line. The + layer overlaps little with the closed magnetic field region. This structure is consistent with the result that the outer part of the quiet arcs corresponds to open magnetic field lines (Tanaka, Ebihara, et al., 2019; Tanaka et al., 2021). In Figure 1, the high-latitude part of + shear⑤ distributes differently from the low-latitude part③. Within intensities drawn here, the high-latitude part⑤ is not visible in the distant tail. The extending part③ is distinct only at the low-latitude edge of the region-1 FAC. This part is generally called the pre-onset arc, where the initial substorm signature is observed (Jiang et al., 2012; Wu et al., 2017). The high-latitude part will correspond to the chain row of the inverted V. These results indicate that the substorm starting point is in the upward FAC part that can be most severely influenced by the plasma sheet disturbance. Thus, it is quite natural to observe the onset that starts from the equatorward-most quiet arc, i.e., the pre-onset arc.

In Figure 1, the magnetic field line (white line) is not always in the same meridional plane as the contour lines, so the relative position of the + layer in the northern hemisphere and the first open magnetic field line is somewhat unclear in the oblique view. To make it clearer, Figure 2 shows the three-dimensional structure of the plasma sheet. The green surface is the iso-pressure surface that depicts the surface corresponding to the open/closed (O/C) boundary in the tail or the lobe-plasma sheet boundary. This figure is viewed from a little tailward of the $+Y$ axis so that the + layer in the northern hemisphere and the position of magnetic field lines can be seen clearly. Due to the IMF By, the plasma sheet is slightly tilted to the $-Z$ direction on the evening side and to $+Z$ direction on the morning side. Nevertheless, it can be confirmed from this figure that the northern hemispheric + layer and first open magnetic field lines are along the surface of the plasma sheet. As explained below, these structures show that + Vy is maximized at the plasma sheet surface. Such a flow structure over mid- and inner-tail regions is a global extension of shear structure that drives the quiet arc shown by Tanaka, Ebihara, et al. (2017) and Tanaka et al. (2021).

3.2. Convection Cells

We call an arrangement in the YZ plane the north-south antisymmetric when the northern and southern structures become the same after rotated 180° around the X axis. We call it asymmetric when they do not have the same shape after the rotation. In the presence of the IMF By, convection in the magnetosphere is almost antisymmetric in the YZ plane (Tanaka, Ebihara, et al., 2017; Tanaka et al., 2021). In the YZ plane under the IMF $By-$, evening convection cell dominates in the northern hemisphere and morning convection cell dominates in the southern hemisphere. In the meridian plane near midnight, the northern

hemisphere is occupied by the evening magnetospheric convection cell and the southern hemisphere is occupied by the morning magnetospheric convection cell.

As estimated by Tanaka, Ebihara, et al. (2017), the growth phase shear that produces the quiet arc is a part of the convection pattern. This convection does not reach the center of the plasma sheet but mainly passes through the surface of the plasma sheet as returns toward the day side. Consequently, convection forms shear along the surface. The HR develops in the northern hemisphere at the footprint of magnetic field lines that go round this shear layer (Tanaka, 2015; Tanaka et al., 2021). Thus, shear layer is a part of the global structure that widely occupies the magnetosphere. This study shows the *XZ* plane structure of shear, in addition to these *YZ* plane structures shown previously. The present result makes it clearer that shear is a connecting structure from the magnetosphere to the ionosphere.

In the growth phase, the *Vy* component and its shear that affect the FAC connection to the ionosphere are also north-south antisymmetric in the *YZ* plane (Tanaka, Ebihara, et al., 2017; Tanaka et al., 2021). Thus, the + layer is dominant near midnight in the northern hemisphere due to the IMF *By*−. In Figure 1, the + layer in the northern hemisphere belongs to the evening cell. This + layer is on the high-latitude side of the flow peak (mainly + *Vy* component). This shear corresponds to the upward region-1 FAC (normal part). The + layer in the southern hemisphere in Figure 1 in the closed magnetic field region belongs to the morning cell. This layer is on the low-latitude side of the flow peak (mainly -Vy component). This shear corresponds to the upward region-2 FAC (extended part). It is also clear in Figure 2 that the + layer in the southern hemisphere is in the closed magnetic field region in the plasma sheet.

In the northern hemisphere, a prominent − layer is also distributed on the equator side of the + layer. It exists in the closed magnetic field region and is not connected to the mid-tail. These + and − layers are on the high-latitude and low-latitude sides of the flow peak (mainly + Vy component). In the ionosphere, this - layer connects to the region-1/2 FAC boundary and to the downward region-2 FAC. The - layer in the southern hemisphere is on the high-latitude side of the + layer, although it is quite thin. The FAC structure becomes complicated here (at LT 23) because its meridional position is near the boundary between the morning and evening cells in the southern hemisphere. The region-1 FAC is weak because it is close to the boundary between the evening structure, which has the upward FAC on the poleward side, and the morning structure, which has the downward FAC on the poleward side.

3.3. NENL Onset (Second Stage)

In the convection-driven substorm, the evolution of the null-separator structure during the growth phase results in the NENL formation through the guide field reconnection (Tanaka, Ebihara, et al., 2019). Figure 3 shows the appearance of new shear structure in the middle tail at the NENL formation ($T = -2.8$ min = start of the second stage). The format of this figure is the same as Figure 1. A blue line is the first open magnetic field line. Shear structure in the NENL region in the middle tail begins to exhibit a completely different pattern that is characterized by a quadrupole configuration① in the *XZ* plane. This structure is almost antisymmetric in the *XZ* plane. The antisymmetry in the *XZ* plane reflects the excitation process of *Vy* associated with the NENL. These patterns seen in Figure 3 are clearly different from shear dynamics in Figure 1 which reflects growth phase convection③⑤. In shear generated by the NENL, the new + layer on the +*Z* side prevails on the earth side and the new + layer on the −*Z* side prevails on the tail side. In Figure 3, the new + layer on the +Z side is on the way to extend to the northern ionosphere②. It is apparent from Figure 3 that this extending part is on a closed magnetic line. In this way, the substorm disturbance in the second stage proceeds accompanied by new magnetospheric shear that is extending from the NENL to the ionosphere along the closed field line.

In this study, the second stage is investigated in the pre-midnight region. At the timing of Figure 3, onset convection cannot be antisymmetric since the NENL is at 23 LT and does not reach 1 LT. In the southern hemisphere, overlapping of onset structure and evening-morning boundary position makes the problem complicated. Near the ionosphere, shear structure③⑤ still has not changed significantly even at the start of the second stage (Figure 3). In both hemispheres, the + layer exists as unchanged from the first stage. Although not displayed, morning side (1 LT) shear also has not changed significantly, because this LT is still not affected by the NENL. Thus, the onset dynamics are not north-south antisymmetric. Dynamics of the

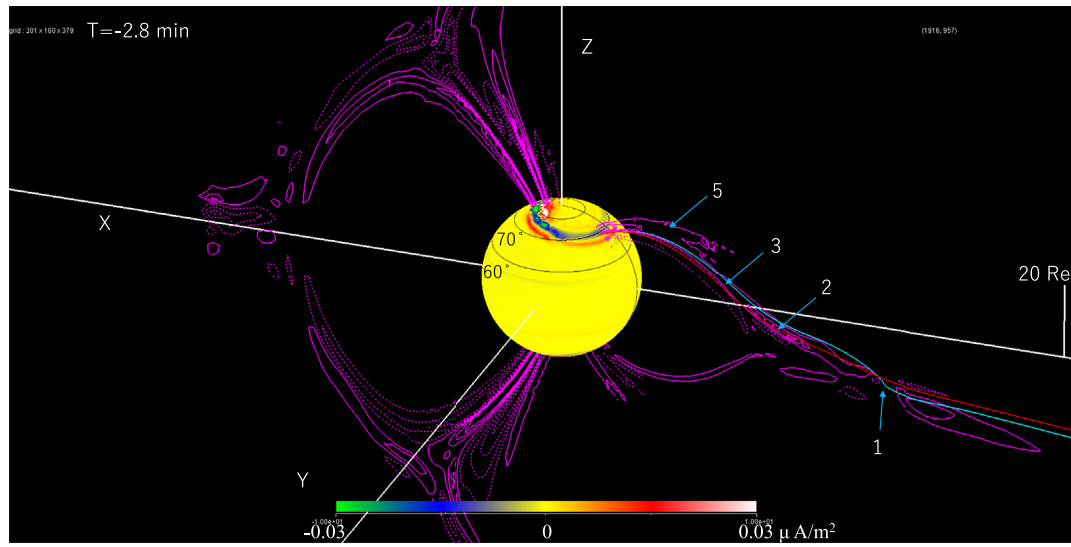

Figure 3. Shear structures in the 12 LT and 23 LT meridian planes at the near-earth neutral line (NENL) onset at $T = -2.8$ min (magenta contour). Solid and dashed contours illustrate + and − layers, respectively. Color shadings show the field-aligned current (FAC) on the 3 Re spherical surface. Black circles show the projected ionospheric latitudes. Upward FAC (blue) is extending from the evening to midnight in the northern hemisphere. A blue line shows the first open field line near the 23 LT meridian. The NENL formation is observable from contours on the nightside. The new + shear extends from the NENL on a closed field line. See encircled numbers in the text for the meaning of numbers.

HR is also investigated mainly in the hemisphere where the HR prevails (Tanaka et al., 2021). In general, the analysis of the HR in the opposite hemisphere has not progressed so much. The lack of the north-south antisymmetry in the HR will be related to such structure. In addition, the formation of the HR is expected to include the effect of the Hall current (Tanaka, 2001). This effect also prevents the north-south antisymmetry. These compound processes will require future tasks.

Flow and shear extending from the NENL are clearly the phenomena within closed magnetic field lines. Most of the quiet arcs expected in Figures 1 and 2 are on open field lines (Tanaka, Ebihara, et al., 2019; Tanaka et al., 2021). Therefore, the result in Figure 3 that the new + layer extending from the NENL occurs in the region of the closed magnetic field can explain the onset that starts from the equatorward-most quiet arc (=pre-onset arc) or from more equatorward. As seen in Ebihara and Tanaka (2015b) and Tanaka, Ebihara, et al. (2017), this feature is consistent with the onset model in which the near-earth dynamo induced by dynamical process connected to the NENL causes the onset. From Figure 3, therefore, it can be concluded that the onset proceeds with flow dynamics including the replacement of flow shear.

Figure 4 shows three-dimensional shear structure by adding isosurfaces of shear to the result in Figure 3. Isosurfaces in Figure 4 show three-dimensional shear distribution for 20-4 LT in the northern hemisphere. From this three-dimensional structure, many more interesting results are observable. The + (orange)① and − (green)② layers that have appeared during the growth phase can still be observable form isosurfaces near the ionosphere. It is observable even from shear drawn for 20-4 LT in Figure 4 that these layers extend in the east-west direction. This corresponds to the extension of the quiet arc in the east-west direction. At the LT near the NENL, on the other hand, there appears local shear excited by the NENL and a narrow structure (orange) extending from the NENL to the ionosphere③. It is seen from Figure 4 that the narrow + layer extending from the NENL reaches as far as the ionosphere even just after the NENL onset. However, it does not mean that no shear is excited outside the narrow structure but strong shear is presented on the narrow structure. This structure is a necessary condition for the onset FAC that connects to the ionosphere at a narrow point. Such thin shear extending to the ionosphere should exist even in the substorm that considers the CW, since it is inevitable to connect the FAC to the ionosphere.

The difference in shape between the wide east-west structure and the extending narrow structure depends on the origin of shear. The former is a part of global convection, and the latter is a more instantaneous and

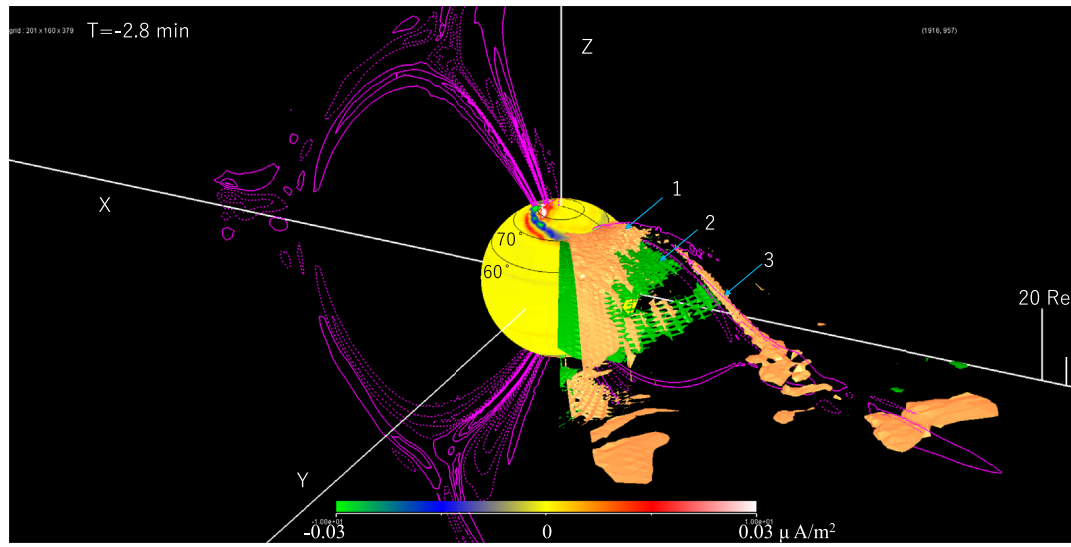

Figure 4. The same drawing as Figure 3 but with additional contour surfaces of shear layers ($\pm 5*10^{1/2}/120$ [nT]$^{1/2}$/sec, orange + and green −). The contour surfaces are drawn for 20-04 LT. Color shadings show the field-aligned current on the 3 Re spherical surface. Black circles show the projected ionospheric latitudes. A narrow shear extends from the near-earth neutral line replacing wide shears formed during the growth phase. See encircled numbers in the text for the meaning of numbers.

local structure generated by the NENL. Tanaka, Ebihara, et al. (2017) reported the development of this narrow structure at the onset as time variations of *Vy* and *Vz*. These results show that convection flow seems to penetrate from the lobe to the plasma sheet along a magnetic field line connected to the NENL. This invasion proceeds from the mid-tail to the near-earth tail as an extension of reconnection flow (We call it direct penetration flow). Movie M3 ($T = -5.9$–0 min) in the Supporting Information visualizes the direct penetration flow V. The extending narrow structure in Figure 4 corresponds to rotation (rot.V) of the invasion motion seen in the movie. In addition, Ebihara and Tanaka (2015b) showed a vector representation of flow structure in this narrow region. The vector representation clearly showed that penetrating flow forms a vortex structure in the course of entering from the lobe to the plasma sheet.

The present result suggests that the pre-existing growth phase shear is affected to some extent by the NENL formation and the replacement of shear structure. It can be seen by comparing Figures 1 and 4 that a part of growth phase + shear on the tail side of the NENL disappears after NENL formation. It also seems in Figure 4 that two types (wide and narrow) of shear layer interact with each other. This result is applicable to the phenomenon that the quiet arc temporarily fades out before the ground onset. This phenomenon has been known for a long time. Until now, many speculations have been proposed for the cause of this phenomenon (Coxon et al., 2017). The structural difference in Figures 1 and 3 may be related to this phenomenon. It is presumed that pre-existing shear weakens before the completion of shear replacement. Such weakening may temporarily make the quiet arc darken until the arrival of narrow shear structure.

3.4. Ground Onset

Contour lines in Figure 5 show shear distributions in the 12 LT and 23 LT meridian planes at the ground onset ($T = 0$ min). Inset in the left bottom part shows the FAC distribution seen from the north. A blue line is the first open magnetic field line in the 23 LT meridian plane. At this time, a spot-like increase corresponding to the initial brightening is observed in the region-1 FAC in the ionosphere (colors shadings). In the northern hemisphere, the + layer① increases its strength and extends from the NENL to the ionospheric upward region-1 FAC along a closed magnetic field, while the –layer② on the more equatorward side also increases its strength and leads to the downward region-2 FAC. The + layer connected to the onset FAC is a clockwise vortex when viewed toward the direction of the magnetic field. All of these onset processes occur

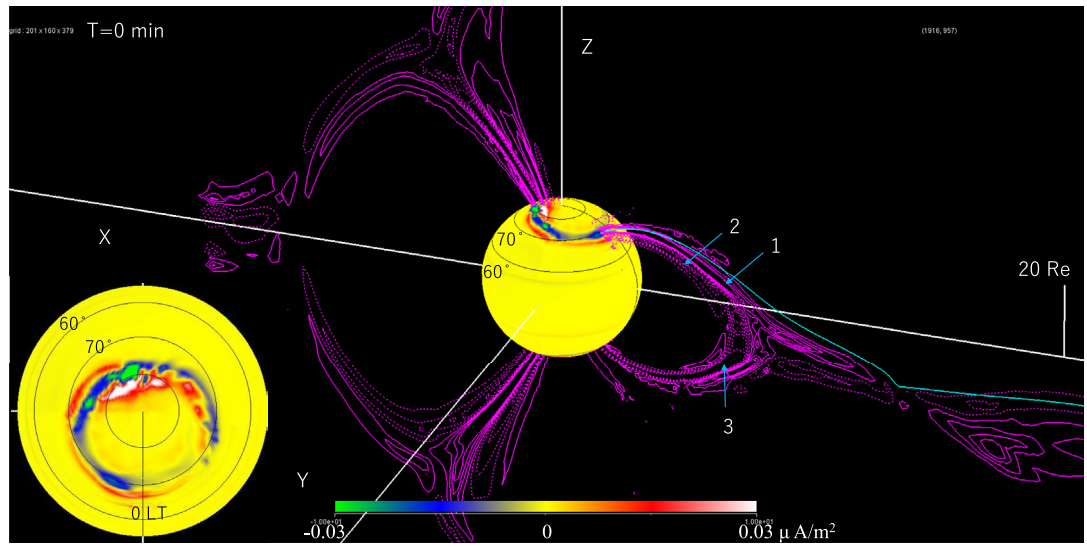

Figure 5. Shear structures in the 12 LT and 23 LT meridian planes at the ground onset at $T = 0$ min (magenta contour). Solid and dashed contours illustrate + and − layers, respectively. Color shadings show the field-aligned current (FAC) on the 3 Re spherical surface. Black circles show the projected ionospheric latitudes. The onset FAC is observable on the northern ionosphere at 23 T. A blue line shows the first open field line near the 23 LT meridian. Inset in the left bottom part shows the FAC distribution seen from the north. See encircled numbers in the text for the meaning of numbers.

along a closed magnetic field as seen from a blue line in Figure 5. These events correspond to the end of the second stage.

While + shear strength becomes dominant in the northern hemisphere, − shear becomes dominant in the southern hemisphere③. The northern + and southern − layers increase their strength during the onset and reach the ionosphere at the time of the ground onset. The − layer in the southern hemisphere connects to the downward region-1 FAC extending from post-midnight. Unlike the structure of the growth phase, the southern + layer becomes weaker. As a consequence, pre-existing growth phase shear (almost) in the open magnetic field is replaced by shear extending from the NENL along the closed magnetic field. In the tail, the northern + layer and southern − layer are both within the closed magnetic field line and are close to each other. This structure corresponds to the convection return path that has changed to the center of the plasma sheet. This process occurs under dynamic shrinking of magnetic field structure and change of magnetic configuration recognized as the DF (Tanaka, Ebihara, et al., 2017; Tanaka et al., 2010, 2021).

In the southern hemisphere, the extending − layer is not directly connected to the NENL in this meridian. This − layer in the southern hemisphere is near the boundary between the evening structure which has the upward FAC on the poleward side and the morning structure which has the downward FAC on the poleward side. Therefore, the onset region-1 FAC (upward) is close to the morning region-1 FAC (downward). This arrangement is realized because the onset in the southern hemisphere occurs in the morning cell that is extending to the evening over midnight (Bristow, 2009; Grocott et al., 2010). This is in contrast to the northern hemisphere where the onset occurs deep within the upward FAC region because the boundary between evening/morning structures lies far from the onset LT. The onset in the southern hemisphere is not antisymmetric to the northern hemisphere. Furthermore, the two cells convection in the expansion phase cannot be antisymmetric since the westward traveling sure (WTS) moves toward the evening both in the northern and southern hemispheres. As a result, the onset in the southern hemisphere becomes complicated. The structure near the boundary is not yet well understood at the present time. It will be a future issue to clarify the overlapping structure for these boundaries and the southern onset.

Figure 6 shows the three-dimensional distribution of the near-earth dynamo (green isosurface for $J \cdot E$) and current lines (red and magenta) in addition to contours and shadings drawn in Figure 5. It was shown by Ebihara and Tanaka (2015b) that the near-earth dynamo, which generates the onset FAC, forms in the

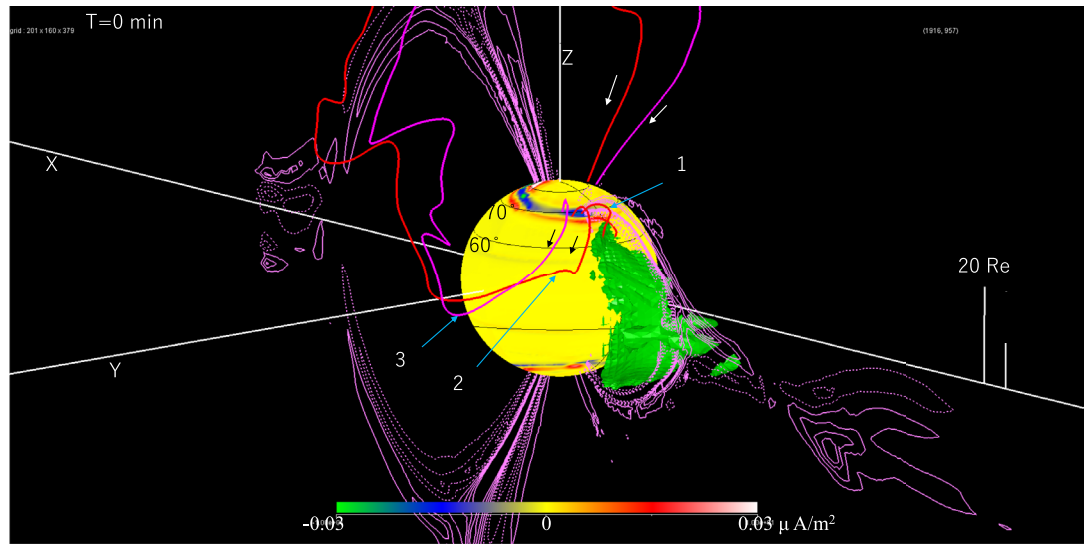

Figure 6. The same drawing as Figure 5 but with an additional contour surface (20×10^{-13} joule/sec/m^3) of the near-earth dynamo (green). Red and magenta lines are the onset field-aligned current (FAC) traced from the onset point and the region-1 FAC traced from the preexisting quiet arc. Color shadings show the FAC on the 3 Re spherical surface. See encircled numbers in the text for the meaning of numbers.

inner magnetosphere away from the equatorial plane. The green isosurface in Figure 6 corresponds to this dynamo. The location of this dynamo in the northern hemisphere is on the earthward side of the NENL. It is around the − layer extending to the ionosphere along with the region-2 FAC. The corresponding + layer in the southern hemisphere is not clearly visible as it is behind the isosurface. The region-1 FAC (red line①) connected to the center of the onset point extends upward along the + layer, bends at the near-earth dynamo, transfers to the − layer, and then connects to the earth along the − layer as the region-2 FAC. Therefore, not only the region-1 FAC but also the region-2 FAC will increase simultaneously at the onset (Coxon et al., 2017). The upward onset FAC at the edge of the onset region (red line②) includes a component that is bent by the near-earth dynamo and directly connected to the westward tail current (Tanaka, 2015). The current line (magenta line) extending from the preexisting quiet arc is also connected to the westward tail current. However, in the case of the magenta line③, it does not include sudden bent but gradually turns and leads to a westward tail current.

During the expansion phase, thin shear extending from the NENL in Figure 4 widens, and the increased region-1 FAC behind the WTS is connected to the cusp-mantle dynamo through the flank magnetopause. Subsequently, the near-earth dynamo disappears, and direct penetration flow grows to sunward return flow that passes through the center of the plasma sheet (Tanaka, Ebihara, et al., 2017). Expansion phase convection is constructed from this flow, strengthened shear between the sunward flow in the ring current region and the lobe anti-sunward flow, the strengthened region-1 and 2 FACs, the cusp-mantle dynamo (for region 1), and the dynamo in the inner plasma sheet (for region 2). Thus, the onset FAC is a transient phenomenon in the process of replacing convection.

4. Conclusion

This study showed that the substorm is a manifestation of global reconfiguration of the convection system. The substorm progresses with the development of convection. To show this process, this paper investigated shear connecting the magnetosphere and the ionosphere, and the FAC connecting the magnetsphere and the ionosphere, simultaneously. The growth phase interval until the onset of the NENL is defined as the first stage and the period from the NENL formation to the ground onset as the second stage. Results of the analysis were shown for the case of the IMF By–where evening convection cell prevails in the northern hemisphere. In the substorm sequence, the quiet arc and the onset occur by the activity of the FAC. In this paper, the FAC develops with the dynamo and leads to the ionosphere through shear. These shear structures

are apparently a part of the global convection. The onset FAC is develops associated with the transition in the convection system (Tanaka, Ebihara, et al., 2017).

In the first stage, significant convection shear is formed along the O/C boundary just the outer and inner sides of the plasma sheet surface. Outer shear is a structure that continues over a long distance from the middle tail to the HR, showing that it is a part of the global dynamics. Near midnight in the northern hemisphere, this shear corresponds to the region-1 FAC (upward at midnight in the northern hemisphere) indicating that the quiet arc is linked to global dynamics. It is misleading to explain the quiet arc by a local mechanism such as particle scattering. Inner shear corresponds to the region-2 FAC (downward in the midnight northern hemisphere) that leads to the partial ring current.

The primary cause of the second stage is the dynamic replacement of flow from the growth phase convection to the expansion phase convection (Tanaka, Ebihara, et al., 2017). It is the growth phase convection that builds up the condition for transition (Tanaka, Ebihara, et al., 2019). The ground onset starts from transient local dynamics brought about by the NENL. Along a closed field line extending from the NENL to the ionosphere, there occur direct penetration flow V in the midway, narrow shear (rot V) propagating toward the ionosphere, increase in pressure P due to the squeezing, formation of the near-earth dynamo, and the release of the HR on the ground (Tanaka et al., 2021). Narrow shear propagates parallel to the magnetic field and replaces the growth phase shear. It reaches the near-earth region earlier than the BBF that propagates in the equatorial plane perpendicular to the magnetic field.

In the global simulation, the CW that is triggered by the BBF is not the cause of the ground onset. The near-earth dynamo causes the ground onset at the same time of arrival of narrow shear. In this dynamics, the near-earth dynamo ($J \bullet E < 0$) is formed from E (determined from V as $E + V \times B = 0$) and J (determined from P as $J \times B = \nabla P$) (Tanaka, Ebihara, et al., 2017). The onset FAC is generated by the near-earth dynamo and guided by narrow shear-induced from the NENL. In this way, aurora switches from the quiet arc along open magnetic field to the onset arc along closed magnetic field. Narrow shear and the FAC grow to global scale convection in the expansion phase. It is too easy to explain the onset by adopting the CW triggered by the BBF.

Data Availability Statement

Numerical data https://doi.org/10.17592/002.2020100389, coordinate data and variable data, information for graphic program and history data necessary to reproduce drawings, are available at https://scidbase.nipr.ac.jp/modules/metadata/index.php?content_id=389/ and at the rink from it http://polaris.nipr.ac.jp/~reppu/reppu2/2020b_she_v01/.

Acknowledgments
In the present study, the authors used the high-speed computing system at Polar Data Center of National Institute of Polar Research through General Collaboration Project 2–3, the KDK computer system at the Research Institute for Sustainable Humanosphere (RISH), Kyoto University through General Collaboration Project R2-KDK-03, and Nagoya University super computer system through Nagoya University High Performance Computing Research Project for Joint Computational Science in Japan. This study was supported by KAKENHI (JSPS KAKENHI Grant Number JP20H01960, Y. Ebihara) and KAKENHI (JSPS KAKENHI Grant Number JP20K03894, M. Watanabe).

References

Birn, J., & Hesse, M. (2013). The substorm current wedge in MHD simulations. *Journal of Geophysical Research: Space Physics*, *118*, 3364–3376. https://doi.org/10.1002/jgra.50187

Bristow, W. A. (2009). Relationship between substorm onset locations and nightside convection pattern features. *Journal of Geophysical Research*, *114*, A12202. https://doi.org/10.1029/2009JA014576

Coroniti, F. V., & Pritchett, P. L. (2014). The quiet evening auroral arc and the structure of the growth phase near-Earth plasma sheet. *Journal of Geophysical Research: Space Physics*, *119*, 1827–1836. https://doi.org/10.1002/2013JA019435

Coxon, J. C., Rae, I. J., Forsyth, C., Jackman, C. M., Fear, R. C., & Anderson, B. J. (2017). Birkeland currents during substorms: Statistical evidence for intensification of Regions 1 and 2 currents after onset and a localized signature of auroral dimming. *Journal of Geophysical Research: Space Physics*, *122*, 6455–6468. https://doi.org/10.1002/2017JA023967

Ebihara, Y., & Tanaka, T. (2015a). Substorm simulation: Formation of westward traveling surge. *Journal of Geophysical Research: Space Physics*, *120*, 10–466. https://doi.org/10.1002/2015JA021697

Ebihara, Y., & Tanaka, T. (2015b). Substorm simulation: Insight into the mechanisms of initial brightening. *Journal of Geophysical Research: Space Physics*, *120*, 7270–7288. https://doi.org/10.1002/2015JA021516

Ebihara, Y., & Tanaka, T. (2016). Substorm simulation: Quiet and N-S arcs preceding auroral breakup. *Journal of Geophysical Research: Space Physics*, *121*, 1201–1218. https://doi.org/10.1002/2015JA021831

Ebihara, Y., & Tanaka, T. (2017). Energy flow exciting field-aligned current at substorm expansion onset. *Journal of Geophysical Research: Space Physics*, *122*, 12228–12312. https://doi.org/10.1002/2017JA024294

Ebihara, Y., Tanaka, T., & Kamiyoshikawa, N. (2019). New diagnosis for energy flow from solar wind to ionosphere during substorm: Global MHD simulation. *Journal of Geophysical Research: Space Physics*, *124*. https://doi.org/10.1029/2018JA026117

Ebihara, Y., Tanaka, T., & Kikuchi, T. (2014). Counter equatorial electrojet and overshielding after substorm onset: Global MHD simulation study. *Journal of Geophysical Research: Space Physics*, *119*, 7281–7296. https://doi.org/10.1002/2014JA020065

Grocott, A., Milan, S. E., Yeoman, T. K., Sato, N., Yukimatu, A. S., & Wild, J. A. (2010). Superposed epoch analysis of the ionospheric convection evolution during substorms: IMF BY dependence. *Journal of Geophysical Research*, *115*, A00I06. https://doi.org/10.1029/2010JA015728

Iijima, T. (2000). Field-aligned currents in geospace: Substance and significance, In S.-I. Ohtani, R. Fujii, M. Hesse, & R. L. Lysak (Eds.), *Magnetospheric current systems, Geophysical Monograph Series*. (Vol. 118, pp. 107–129): AGU. https://doi.org/10.1029/gm118p0107

Iijima, T., & Potemra, T. A. (1976). Field-aligned currents in the dayside cusp observed by Triad. *Journal of Geophysical Research*, *81*(34), 5971–5979. https://doi.org/10.1029/JA081i034p05971

Jiang, F., Strangeway, R. J., Kivelson, M. G., Weygand, J. M., Walker, R. J., Khurana, K. K., et al. (2012). In situ observations of the "pre-existing auroral arc" by THEMIS all sky imagers and the FAST spacecraft. *Journal of Geophysical Research*, *117*, A05211. https://doi.org/10.1029/2011JA017128

Johnson, J. R., & Wing, S. (2015). The dependence of the strength and thickness of field-aligned currents on solar wind and ionospheric parameters. *Journal of Geophysical Research: Space Physics*, *120*, 3987–4008. https://doi.org/10.1002/2014JA020312

Kepko, L., McPherron, R. L., Amm, O., Apatenkov, S., Baumjohann, W., Birn, J., et al. (2015). Substorm current wedge revisited. *Space Science Review*, *190*, 1–46. https://doi.org/10.1007/s11214-014-0124-9

Kikuchi, T. (2014). Transmission line model for the near-instantaneous transmission of the ionospheric electric field and currents to the equator. *Journal of Geophysical Research: Space Physics*, *119*, 1131–1156. https://doi.org/10.1002/2013JA019515

Liu, J., Angelopoulos, V., Chu, X., Zhou, X.-Z., & Yue, C. (2015). Substorm current wedge composition by wedgelets. *Geophysical Research Letters*, *42*, 1669–1676. https://doi.org/10.1002/2015GL063289

Lui, A. T. Y., Angelopoulos, V., LeContel, O., Frey, H., Donovan, E., Sibeck, D. G., et al. (2008). Determination of the substorm initiation region from a major conjunction interval of THEMIS satellites. *Journal of Geophysical Research: Space Physics*, *113*, A00C04. https://doi.org/10.1029/2008JA013424

Lyons, L. R., Liu, J., Nishimura, Y., Reimer, A. S., Bristow, W. A., Hampton, D. L., et al. (2021). Radar observations of flows leading to substorm onset over Alaska. *Journal of Geophysical Research: Space Physics*, *126*, 2. https://doi.org/10.1029/2020JA028147

McPherron, R. L. (2016). Where and when does reconnection occur in the tail? *Journal of Geophysical Research: Space Physics*, *121*, 4607–4610. https://doi.org/10.1002/2015JA022258

McPherron, R. L., El-Alaoui, M., Walker, R. J., & Richard, R. (2020). Characteristics of reconnection sites and fast flow channels in an MHD Simulation. *Journal of Geophysical Research: Space Physics*, *125*. https://doi.org/10.1029/2019JA027701

Nakamizo, A., Tanaka, T., Kubo, Y., Kamei, S., Shimazu, H., & Shinagawa, H. (2009). Development of the 3-D MHD model of the solar corona-solar wind combining system. *Journal of Geophysical Research*, *114*, A07109. https://doi.org/10.1029/2008JA013844

Nishimura, Y., & Lyons, L. R. (2016). Localized reconnection in the magnetotail driven by lobe flow channels: Global MHD simulation. *Journal of Geophysical Research: Space Physics*, *121*, 1327–1338. https://doi.org/10.1002/2015JA022128

Ohtani, S., Gkioulidou, M., Wang, C.-P., & Wolf, R. A. (2016). The Harang reversal and the interchange stability of the magnetotail. *Journal of Geophysical Research: Space Physics*, *121*, 3278–3292. https://doi.org/10.1002/2015JA022025

Pham, K. H., Lopez, R. E., & Bruntz, R. (2016). The effect of a brief northward turning in IMF Bz on solar wind magnetosphere coupling in a global MHD simulation. *Journal of Geophysical Research: Space Physics*, *121*, 4291–4299. https://doi.org/10.1002/2015JA021982

Raeder, J., McPherron, R. L., Frank, L. A., Kokubun, S., Lu, G., Mukai, T., et al. (2001). Global simulation of the Geospace Environment Modeling substorm challenge event. *Journal of Geophysical Research*, *106*, 381–395. https://doi.org/10.1029/2000ja000605

Sato, T., & Iijima, T. (1979). Primary sources of large-scale Birkeland currents. *Space Science Reviews*, *24*(3), 347–366. https://doi.org/10.1007/BF00212423

Sergeev, V., Nishimura, Y., Kubyshkina, M., Angelopoulos, V., Nakamura, R., & Singer, H. (2012). Magnetospheric location of equatorial prebreakup arc. *Journal of Geophysical Research*, *117*, A01212. https://doi.org/10.1029/2011JA017154

Sergeev, V. A., Angelopoulos, V., & Nakamura, R. (2012). Recent advances in understanding substorm dynamics. *Geophysical Research Letters*, *39*, L05101. https://doi.org/10.1029/2012GL050859

Song, Y., & Lysak, R. L. (2001). The physics in the auroral dynamo regions and auroral particle acceleration. *Physics and Chemistry of the Earth—Part C: Solar, Terrestrial & Planetary Science*, *26*(1–3), 33–42. https://doi.org/10.1016/S1464-1917(00)00087-8

Sorathia, K. A., Merkin, V. G., Panov, E. V., Zhang, B., Lyon, J. G., Garretson, J., et al. (2020). Ballooning-interchange instability in the near-Earth plasma sheet and auroral beads: Global magnetospheric modeling at the limit of the MHD approximation. *Geophysical Research Letters*, *47*, e2020GL088227. https://doi.org/10.1029/2020GL088227

Tanaka, T. (1994). Finite volume TVD scheme on an unstructured grid system for three-dimensional MHD simulation of inhomogeneous systems including strong background potential fields. *Journal of Computational Physics*, *111*(2), 381–389. https://doi.org/10.1006/jcph.1994.1071

Tanaka, T. (1995). Generation mechanisms for magnetosphere-ionosphere current systems deduced from a three-dimensional MHD simulation of the solar wind-magnetosphere-ionosphere coupling processes. *Journal of Geophysical Research*, *100*(A7), 12057–12074. https://doi.org/10.1029/95JA00419

Tanaka, T. (2000). The state transition model of the substorm onset. *Journal of Geophysical Research*, *105*, 21081–21096. https://doi.org/10.1029/2000JA900061

Tanaka, T. (2001). IMF By and auroral conductance effects on high-latitude ionospheric convection. *Journal of Geophysical Research*, *106*–24516–24505. https://doi.org/10.1029/2001JA900061

Tanaka, T. (2007). Magnetosphere-ionosphere convection as a compound system. *Space Science Reviews*, *133*, 1–72. https://doi.org/10.1007/s11214-007-9168-4

Tanaka, T. (2015). Substorm auroral dynamics reproduced by the advanced global M-I coupling simulation. In Y. Zhang (Ed.), *Auroral dynamics and space weather, Geophysical Monograph Series* (Vol. 215, pp. 177–190): AGU. https://doi.org/10.1002/9781118978719.ch13

Tanaka, T., Ebihara, Y., Watanabe, M., Den, M., Fujita, S., Kikuchi, T., et al. (2017). Global simulation study for the time sequence of events leading to the substorm onset. *Journal of Geophysical Research: Space Physics*, *122*, 6210–6239. https://doi.org/10.1002/2017JA024102

Tanaka, T., Ebihara, Y., Watanabe, M., Den, M., Fujita, S., Kikuchi, T., et al. (2019). Development of magnetic topology during the growth phase of the substorm inducing the onset of the near-earth neutral line. *Journal of Geophysical Research: Space Physics*, *124*. https://doi.org/10.1029/2018ja026386

Tanaka, T., Ebihara, Y., Watanabe, M., Den, M., Fujita, S., Kikuchi, T., et al. (2020). Reproduction of ground magnetic variations during the SC and the substorm from the global simulation and Biot-Savart's law. *Journal of Geophysical Research: Space Physics*, *125*, e2019JA027172. https://doi.org/10.1029/2019ja027172

Tanaka, T., Ebihara, Y., Watanabe, M., Den, M., Fujita, S., Kikuchi, T., et al. (2021). Formation and release of the Harang reversal relating with the substorm onset process. *Journal of Geophysical Research: Space Physics*, *125*, 2020JA028170. https://doi.org/10.1029/2020ja028170

Tanaka, T., Nakamizo, A., Yoshikawa, A., Fujita, S., Shinagawa, H., Shimazu, H., et al. (2010). Substorm convection and current system deduced from the global simulation. *Journal of Geophysical Research*, *115*, A05220. https://doi.org/10.1029/2009JA014676

Tanaka, T., Obara, T., Watanabe, M., Fujita, S., Ebihara, Y., & Kataoka, R. (2017). Formation of the Sun-aligned arc region and the void (polar slot) under the null-separator structure. *Journal of Geophysical Research: Space Physics*, *122*, 4102–4116. https://doi.org/10.1002/2016JA023584

Tanaka, T., Obara, T., Watanabe, M., Fujita, S., Ebihara, Y., Kataoka, R., & Den, M. (2018). Cooperatives roles of dynamics and topology in generating the magnetosphere-ionosphere disturbances: Case of the theta aurora. *Journal of Geophysical Research: Space Physics*, *123*. https://doi.org/10.1029/2018ja025514

Tanaka, T., Obara, T., Watanabe, M., Fujita, S., Ebihara, Y., Kataoka, R., & Den, M. (2019). Magnetosphere-ionosphere convection under the due northward IMF. *Journal of Geophysical Research: Space Physics*, *124*. https://doi.org/10.1029/2019ja026547

Tanaka, T., Watanabe, M., Den, M., Fujita, S., Ebihara, Y., Kikuchi, T., et al. (2016). Generation of field-aligned current (FAC) and convection through the formation of pressure regimes: Correction for the concept of Dungey's convection. *Journal of Geophysical Research: Space Physics*, *121*, 8695–8711. https://doi.org/10.1002/2016JA022822

Vasyliunas, V. M. (1970). Mathematical models of magnetospheric convections and its coupling to the ionosphere. In B. M. McCormac (Ed.), *Particles and fields in the magnetosphere* (pp. 60–71): D. Reidel. https://doi.org/10.1007/978-94-010-3284-1_6

Watanabe, M., Tanaka, T., & Fujita, S. (2019). Magnetospheric dynamo driving large-scale Birkeland currents. *Journal of Geophysical Research: Space Physics*, *124*. https://doi.org/10.1029/2018ja026025

Wilder, F. D., Eriksson, S., & Wiltberger, M. (2015). The role of magnetic flux tube deformation and magnetosheath plasma beta in the saturation of the Region 1 field-aligned current system. *Journal of Geophysical Research: Space Physics*, *120*, 2036–2051. https://doi.org/10.1002/2014JA020533

Wu, J., Knudsen, D. J., Gillies, D. M., Donovan, E. F., & Burchill, J. K. (2017). Swarm observation of field-aligned currents associated with multiple auroral arc systems. *Journal of Geophysical Research: Space Physics*, *122*, 10–145. https://doi.org/10.1002/2017JA024439

Yao, Y., Ebihara, Y., & Tanaka, T. (2015). Sudden pressure enhancement and tailward retreat in the near-earth plasma sheet: THEMIS observation and MHD simulation. *Journal of Geophysical Research: Space Physics*, *120*, 201–211. https://doi.org/10.1002/2014JA020482

Yu, Y., Cao, J., Fu, H., Lu, H., & Yao, Z. (2017). The effects of bursty bulk flows on global-scale current systems. *Journal of Geophysical Research: Space Physics*, *122*, 6139–6149. https://doi.org/10.1002/2017JA024168